SCIENCE CHINA Materials ARTICLES

mater.scichina.com link.springer.com

Published online 12 January 2018 | https://doi.org/10.1007/s40843-017-9185-3
Sci China Mater 2018, 61(5): 671–678

WS_2 nanoplates embedded in graphitic carbon nanotubes with excellent electrochemical performance for lithium and sodium storage

Debin Kong[1,2†], Xiongying Qiu[1†], Bin Wang[1], Zhichang Xiao[1], Xinghao Zhang[1], Ruiying Guo[1], Yang Gao[1,2], Quan-Hong Yang[2*] and Linjie Zhi[1*]

ABSTRACT **WS_2 has been considered as a promising anode material due to its high lithium storage capacity as well as fascinating physical properties. However, the insufficient electrical and ionic conductivities deteriorate the rate performance of the batteries. Herein, we report a simple synthetic approach towards graphene-WS_2 hybrids by rolling graphene into a hollow nanotube in which WS_2 nanoplates are encapsulated. This new electrode design strategy facilitates the fabrication of integrated and binder-free lithium ion battery and sodium ion battery electrodes by combining electrospinning and chemical vapor deposition (CVD) methods. Benefiting from their confined growth and the interconnected *in-situ* graphitic carbon coating nanocable web, the WS_2@G with nano-level WS_2 dispersion not only provides an efficiently conductive and electrolyte accessible framework, but effectively alleviates the volume change during the cycling, enabling a mechanically robust binder-free electrode along with the outstanding electrochemical Li^+ and Na^+ storage properties.**

Keywords: two-dimensional materials, lithium-ion battery, sodium-ion battery, core-shell nanocables, binder-free

INTRODUCTION

Very recently, graphene-like two-dimensional (2D) layered materials, such as inorganic transition metal dichalcogenide (TMDC) materials are of great interest for the scientific community due to their unique layered structure and fascinating physical properties [1–3]. Among TMDC, 2D nanoscale metal disulfides, such as MoS_2 [4] and WS_2 [5], have been intensively studied to examine their properties, including electrical transport, luminescence, photocurrent and catalytic properties, as well as their strain effects [6–9]. WS_2, as an important member of the TMDC family, however, has yet been extensively explored in practical applications, and only a few studies have reported that it can be utilized in electrochemical devices such as sodium storage and lithium-ion batteries (LIBs) [10–14]. When used as an anode material for LIBs, the 4-electron transfer reaction hosting lithium ions endowed it with higher lithium storage capacity (443 mA h g^{-1}) than that of a commercial graphite anode (372 mA h g^{-1}) [14,15]. Besides, WS_2 has a larger spacing between neighboring (002) planes (6.18 Å) than that of graphite (3.35 Å), which in principle may make Li^+ diffusion easier [16–18]. Moreover, the density of WS_2 is 7.6 g cm^{-3}, resulting in a high volumetric energy density (about 4 times that of graphite). In spite of these advantages, the insufficient electrical and ionic conductivities derived from their semiconductor characteristics deteriorate the rate performance of the batteries [19,20]. Additionally, though the volume changes are less than those of Si and metal oxides, the large volume changes during the cycling processes usually lead to pulverization and aggregation of particles, and hence poor cycling stability, especially at high discharge/charge rates [21,22]. This is even more important when sodium storage is concerned, which currently attracts much attention because of the limited global resources of lithium.

Several strategies including reducing the size, optimizing the morphology, and incorporating WS_2 into conductive carbonaceous materials, such as graphene [23–25]

[1] CAS Key Laboratory of Nanosystem and Hierarchical Fabrication, CAS Center for Excellence in Nanoscience, National Center for Nanoscience and Technology, Beijing 100190, China
[2] School of Chemical Engineering and Technology, Tianjin University, Tianjin 300072, China
[†] These authors contributed equally to this work.
[*] Corresponding authors (emails: zhilj@nanoctr.cn (Zhi L); qhyangcn@tju.edu.cn (Yang QH))

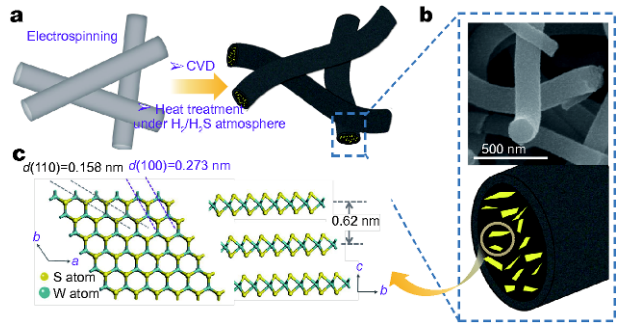

Figure 1 Electrode design. (a) Schematic illustration of the formation procedures; (b) SEM images and scheme of a single nanocable of WS_2@G; (c) top view and side view images of the atomic structures of the layered WS_2 nanoplates.

and carbon nanofibers [20,26] have been proposed to simultaneously deal with the volume expansion problem and provide facile electron pathways, showing enhanced electrochemical performance. Bao *et al.* [27] reported a self-assembled double carbon coating *via* a self-assembly process between oleylamine-coated WS_2 nanosheets and graphene oxide, showing a 90% capacity retention after 200 cycles as well as excellent rate capabilities. Nevertheless, the WS_2-carbonaceous based composites are normally fabricated as powder and thus need to be mixed with excessive additives (e.g., carbon black) and polymer binders, and finally compressed onto a current collector (Al foil) [13,15]. The substantial need of these extra inactive materials adversely affects not only the designated electrochemical properties of the hybrids but also the electrode performance including both volumetric capacity and gravimetric capacity, as the total weight and volume of the electrode must be counted from a practical viewpoint [28-30].

Recently, a new electrode design strategy has been exploited to fabricate integrated and binder-free LIB electrodes by combining electrospinning and chemical vapor deposition (CVD) methods. The resulting framework constructed by graphitic carbon coated nanocables possesses high surface area, skeleton framework and most efficient 1D electron transport pathways [31,32]. The unique graphitic carbon coatings of nanocable can not only facilitate the easy access of electrolyte and the fast transfer of electrons, but also can accommodate the volume changes of metal oxides and sulfides and prevent their aggregation during cycle processes [31,33]. It is also noted that the electron transport of 2D metal disulfides (WS_2) through the basal planes is much faster as compared to the one parallel to the planes [34]. Thus, to encapsulate WS_2 in a graphitic nanocable, especially with side to face contact mode is highly desired.

Herein, as schemed in Fig. 1, we report a facile synthetic approach towards 2D graphene-WS_2 hybrids by rolling graphene into a hollow nanotube in which WS_2 nanoplates are encapsulated. This new electrode design strategy facilitates the fabrication of integrated and binder-free electrodes by combining electrospinning and CVD methods. Due to their confined growth and the interconnected *in-situ* graphitic carbon nanotube web, the resultant few-layer WS_2 nanoplates/graphitic carbon nanotubes (WS_2@G) can effectively alleviate the volume change and the aggregation of WS_2 during the cycling processes, provide an efficiently conductive and electrolyte accessible framework, and additionally enable a mechanically robust binder-free electrode along with the outstanding electrochemical Li^+ and Na^+ storage properties.

EXPERIMENTAL SECTION

Typical procedure for WS_2@G preparation

First, 0.36 g tungsten chloride (WCl_6) was dissolved in 1.5 mL ethanol. A flexible film composed of W-SiO_2-PVP was produced through electrospinning of 4 mL *N*,*N*-dimetylformamide (DMF) solution of 0.65 g polyvinyl pyrrolidone (PVP) with the addition of 1.5 mL ethanol solution of WCl_6 and 500 μL tetraethyl orthosilicate (TEOS). Afterward, the resulting films were conducted through CVD to grow several layers of graphene with good mechanical properties and excellent conductivity, followed by a mild oxidation at 350°C (WO_3-SiO_2@G). Subsequently, WS_2@G was finally obtained by annealing the WO_3-SiO_2@G at 800°C for 2 h in H_2/H_2S and then removal of SiO_2 by HF. The samples containing different WS_2 mass ratio were prepared from electrospinning solutions with different WCl_6 concentrations.

Characterization

The morphologies of the samples were examined by the scanning electron microscopy (SEM, Hitachi S4800) and field emission transmission electron microscopy (FE-TEM, FEI Tecnai G^2 20 ST). Nitrogen adsorption isotherms of the samples were measured with a Micromeritics ASAP 2020 instrument, and the surface area was obtained by Brunauer-Emmett-Teller (BET) analyses. X-ray diffraction (XRD) with Cu Kα radiation (Rigaku D/max-2500B2+/PCX system) was used to determine the phase composition and the crystallinity.

Electrochemical characterization

The free-standing WS_2@G film was directly used as the

working electrode while the working electrode for bulk WS_2 powder was made by active material, acetylene black and poly(vinylidene fluoride) (PVDF) binder (dispersed in *N*-methylpyrrolidone) in a weight ratio of 7:1.5:1.5 on a copper foil. The as-made working electrodes were assembled into coin-type half cells (CR2032) in an argon-filled glovebox (<1 ppm of oxygen and water) with lithium foil as the counter electrode, porous polypropylene film as the separator, and 1 mol L^{-1} $LiPF_6$ in 1:1 (*v*/*v*) ethylene carbonate/diethyl carbonate (EC/DEC) as the electrolyte. Notably, the obtained WS_2@G film was directly used as the electrode without any current collector and binder. For each investigated electrode, the total electrode weight (the weight of WS_2@G film including graphene) was used for calculating specific capacities. The total mass of WS_2@G film applied to each cell was around 1.0 mg cm^{-2}. The cycle-life tests were performed using a CT2001A battery program controlling test system at different current rates within the 3–0.01 V voltage range. Electrochemical measurement of WS_2@G film for Na-ion storage was performed in a half-cell configuration with a Na metal counter electrode and 1 mol L^{-1} $NaClO_4$ in ethylene carbonate and propylene carbonate (EC:PC=1:1 *v*/*v*) electrolyte and 5 wt.% fluoroethylene carbonate additive. The galvanostatic tests were carried out on the Land Battery Measurement System within a voltage range of 10 mV to 3 V. For achieving the capacity value of each electrode material, at least five cells were assembled and characterized under the same conditions. For each investigated electrode, the total electrode weight was used for calculating specific capacities. Electrochemical impedance spectral (EIS) measurements were carried out in the frequency range from 100 kHz to 10 MHz on a Biologic VSP electrochemical workstation.

RESULTS AND DISCUSSION

Fig. 1 shows a schematic illustration of the preparation process and the detailed structure of WS_2@G. In a typical synthesis, a flexible film composed of W-SiO_2@PVP nanocables was obtained through electrospinning of the DMF solution of PVP, tungsten source and TEOS. Afterward, the resulting films were coated with several layers graphitic carbon *via* CVD which provide the structure with good mechanical properties and excellent conductivity after a mild oxidation at 350°C (WO_3-SiO_2@G). Subsequently, WS_2@G was finally obtained by annealing at 800°C in the atmosphere of H_2/H_2S and removing SiO_2 by HF. It is worth mentioning that the contents of WS_2 in the nanocables can be easily tuned by changing the amount of adding W-source.

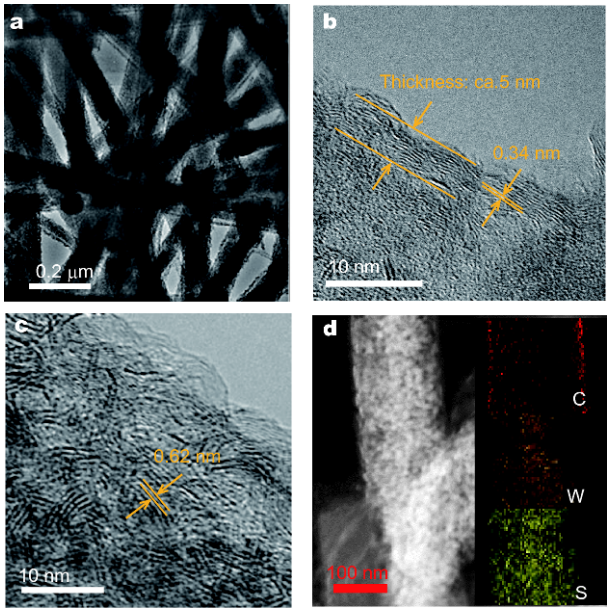

Figure 2 Morphology and microstructure. (a) TEM image of WS_2@G. Scale bar, 0.2 μm. (b, c) HRTEM images of WS_2@G. Scale bar, 10 nm. (d) Dark field transmission electron microscopy image and mapping of WS_2@G. Scale bar, 100 nm.

The self-supported film built up by interwoven nanocables in the as-prepared WS_2@G samples was firstly confirmed by SEM. As shown in Fig. 1b and Fig. S1, the morphologies of the thus-produced hybrid architectures maintained the interwoven nanowires and nanocables network. Each nanocable is around 150 nm in diameter and several micrometers in length. TEM and high-resolution TEM (HRTEM) further confirmed the microstructure of the as-prepared WS_2@G architectures. As presented in Fig. 2a, the continuous and uniform building blocks, nanocables, in interwoven WS_2@G architectures are clearly demonstrated. The typical HRTEM image (Fig. 2b) further discloses the random but firm WS_2 nanoplates core which are encapsulated in the graphitic carbon nanotubes (Fig. S2) with a ca.5 nm thickness of the wall. The characteristic lattice fringe corresponding to 0.62 and 0.34 nm should derive from the (002) lattice of WS_2 and the (001) of multilayer graphitic carbon, respectively (Fig. 2b, c). Coupled with their elemental mapping analysis, the homogeneous distribution of WS_2 in graphitic carbon nanotube is distinctly observed as exhibited in Fig. 2d.

The detailed structure of WS_2@G is further disclosed by XRD and Raman analyses. For comparison, bulk WS_2 powder was adopted and used as an anode material, the morphology of which is shown in Fig. S3. As shown in Fig. 3a, the XRD pattern of the WS_2@G (*P*63/*mmc* space

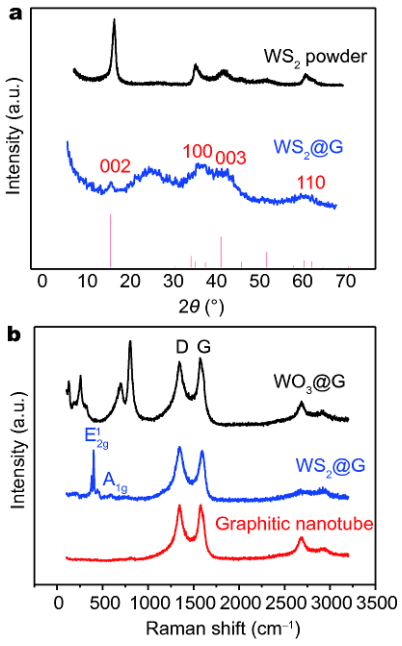

Figure 3 Component analyses. (a) XRD pattern of WS_2@G and WS_2 powder, (b) Raman analysis of WS_2@G and WO_3@G.

group, JCPDS No. 08-0237) is similar to that of the WS_2 powder, the (002) peak for the *c*-axis, the (100) and (110) peaks for the ab-plane. Nevertheless, the obvious broadening of its typical diffraction peaks is attributed to the ultrathin dimension of WS_2 nanoplates [12]. Interestingly, the adsorption data of nitrogen adsorption-desorption curve (Fig. S4) indicates that the specific surface area of WS_2@G is only 12 $m^2 g^{-1}$, reflecting the almost full filling of WS_2 in the cables, which is in consistent with the TEM characterizations.

The Raman scattering spectra of the WS_2@G (Fig. 3b) further confirms that the crystalline WS_2 phase was successfully synthesized. The peak intensity of the out-of-plane vibrational mode (A_{1g}) at 416 cm^{-1} is relatively low compared to that of the in-plane vibrational mode (E^1_{2g}) at 352 cm^{-1} due to the few-layer effect, while for the bulk WS_2 powder, the peak intensity of the A_{1g} mode is comparable to that of the E^1_{2g} mode [35]. The D-band related to the defects and disorder is located at 1,363 cm^{-1}, while the G-band associated with the ordered graphitic crystallites is observed at 1,601 cm^{-1}. The relative intensity ratio of the D-band to the G-band (I_D/I_G) is nearly 1, suggesting that the carbon grown by CVD are not perfect graphene layers but poly-crystalline, defect-containing graphitic carbon structures [36]. Actually, these characters of structure imperfections and defects are critically important for providing multiple pathways for efficient lithium ion transportation as previously reported [37].

The electrochemical properties of the WS_2@G, where the content of WS_2 in the cable is around 70% as confirmed by TGA in Fig. S5, were investigated by cyclic voltammetry (CV) for the initial three cycles over a voltage window of 0.01–3.0 V (*vs.* Li^+/Li) at a scan rate of 0.1 mV s^{-1}, as shown in Fig. S6. A strong cathodic peak located at around 0.56 V can be observed in the first cycle, which is ascribed to the reduction of WS_2 to metallic W embedded in a Li_2S matrix in accompany with the decomposition of the electrolyte. The anodic peak at 2.43 V accounts for the oxidation of W to WS_2. From the 2nd cycle, the original reduction peak at 0.56 V disappears while two smaller cathodic peaks appear at 2.06 and 1.84 V, which correspond to the formation of Li_xWS_2 upon lithium insertion into WS_2, suggesting dramatic lithium driven structural or textural modifications during the first lithiation process [13]. Fig. 4a displays the charge-discharge voltage profiles cycled at a current density of 0.2 A g^{-1} in the same voltage range. The charge and discharge profiles present relatively sloped plateaus, consistent with the broad peaks observed during CV scans. The initial charge and discharge capacities are 502 and 791 mA h g^{-1}, respectively, based on the total mass of the WS_2@G composite. The large initial discharge capacity of the composite is generally ascribed to the production of the solid electrolyte interface (SEI) layer on the surface of the electrode owing to electrolyte decomposition, similar to that reported in nanosized TMD-based anode materials [10,38]. Furthermore, the defect of the graphitic carbon coating with high surface area probably also contributes to this high discharge capacity [23,24]. Despite a large irreversible capacity loss occurred in the first cycle, which is probably due to irreversible Li insertion as well as the formation of an SEI layer on the surface of the WS_2@G electrode, the reversibility of the capacity was greatly enhanced, with an average Coulombic efficiency of nearly 100% for up to 300 cycles after the second cycle (Fig. 4b). Additionally, considering that the capacity of hollow graphitic carbon nanotube is around 370 mA h g^{-1} (Fig. S7), the capacity of WS_2 in the composite is calculated to be 540 mA h g^{-1}.

The stable cycle performance is an essential requirement for a practical anode material. Poor cycle performances of WS_2 powder electrodes are observed in Fig. 4b, which is mainly originated from a structural change and agglomeration of metal sulfides during the conversion reaction. In contrast, our WS_2@G electrodes exhibit ex-

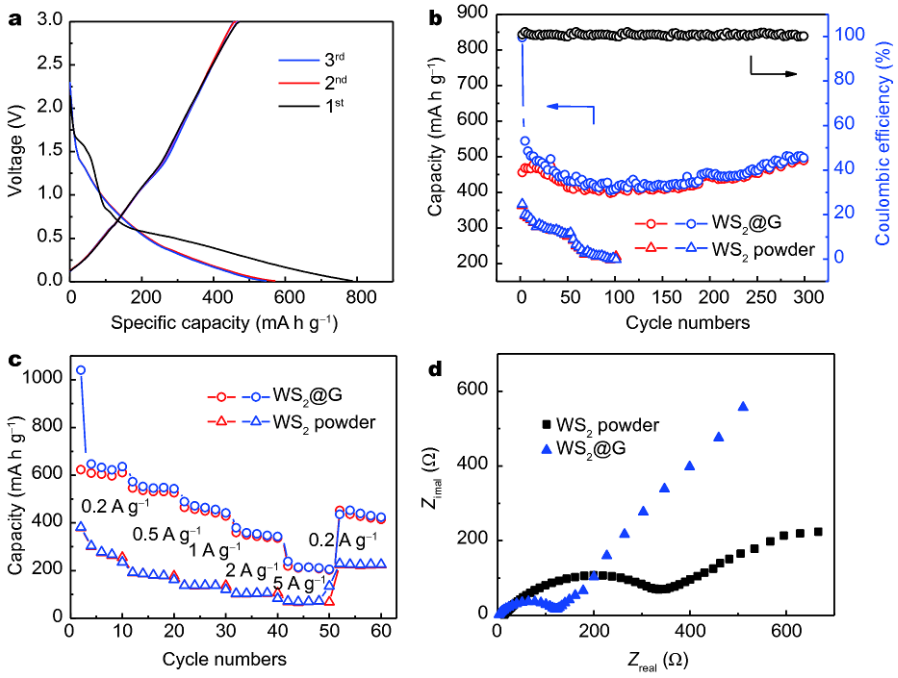

Figure 4 Electrochemical performance of WS_2@G as LIBs anodes. (a) The charge/discharge curves of WS_2@G, (b) cycling performance of WS_2@G and WS_2 powder electrodes under 0.5 A g^{-1}, (c) reversible capacity of WS_2@G and WS_2 powder at various current rates from 0.2 to 5 A g^{-1}, (d) Nyquist plots of the WS_2@G and WS_2 powder.

cellent cycle life and can still deliver a reversible capacity of nearly 500 mA h g^{-1} after 300 cycles at 0.5 A g^{-1}, corresponding to 104.2% capacity retention. The increased capacity in WS_2@G electrode may be attributed to an activation process occurring on conversion reaction [12]. Besides the achieved high specific capacity and superior cycling stability, the WS_2@G electrode shows a satisfactory rate capability as well. As displayed in Fig. 4c, along with increasing current densities from 0.2 to 0.5, 1, 2 and 5 A g^{-1}, reversible capacities of 606, 532, 455, 349, and 211 mA h g^{-1} are achieved, respectively. Importantly, after continuous cycling with the increasing current densities, a specific capacity of as high as 432 mA h g^{-1} could be recovered at a current density of 0.2 A g^{-1}, suggesting an excellent lithium storage reversibility. EIS was implemented to gain in-depth insight of such outstanding electrochemical performance, as shown in the data of the Nyquist plots obtained at a fully lithiated state after 20 cycles (Fig. 4d). Both samples show a semicircle in high to medium frequency regions and an inclined line in low frequency regions, which correspond to the electrochemical reaction impedance (namely, charge transfer) and the ion diffusion impedance, respectively. The much smaller diameter of the semicircle for WS_2@G in the high-medium frequency region indicates the greatly decreased charge-transfer resistance at the electrode/electrolyte interface, while the more vertical line corresponds to the quicker Li^+ diffusion process.

Additionally, the large interlayer gaps between the (002) crystal planes of WS_2 could provide a facile channel for Na ion diffusion and space to accommodate the Na ions, which features the as-prepared WS_2@G a promising electrode candidate for Na-ion batteries (SIBs). The discharge-charge voltage profiles of SIBs are in good agreement with the CV result, and are also similar to those of LIBs. However, the voltage and capacity of SIBs are lower than those of LIBs. The storage reactions of Na have lower absolute values of Gibbs energy change, and the kinetics of Na charging and discharging are more sluggish than those of Li, which can be ascribed to the larger ionic radius of Na^+ than Li^+. Benefiting from the developed conductive networks and unique ion transport channels of 2D materials, the flexible film directly as SIBs anodes exhibits fast sodium storage properties. As shown in Fig. 5, when discharged at altering rates ranging from 50 mA g^{-1} to 3 A g^{-1}, the electrode achieves capacity retention rate of nearly 70% (289 mA h g^{-1} even at a high current density of 3 A g^{-1}). When the current density decreases to 0.1 A g^{-1} after cycling under high current densities, WS_2@G can still regain a reversible capacity

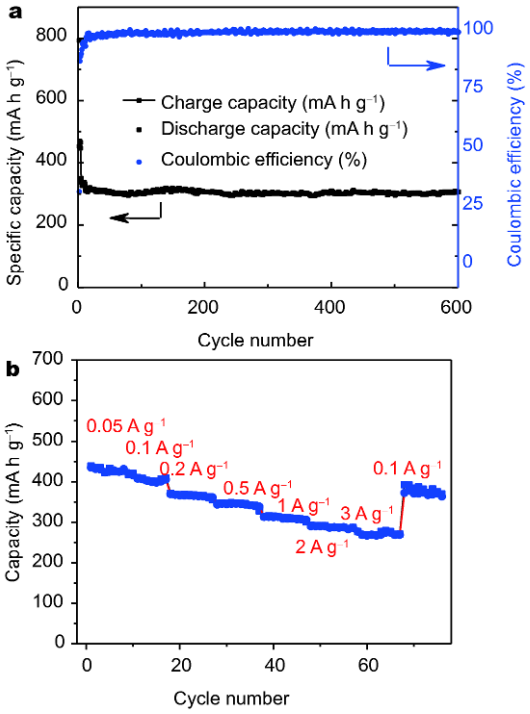

Figure 5 Electrochemical performance of WS_2@G as SIBs anodes. (a) Cycling performance of WS_2@G electrodes under 0.5 A g^{-1}, (b) reversible capacity of WS_2@G at various current rates from 0.05 to 3 A g^{-1}.

near 400 mA h g^{-1}. Except for excellent rate capability, the WS_2@G electrodes deliver excellent Na^+ storage capability with capacity more than 340 mA h g^{-1} when galvanostatically discharging at 500 mA g^{-1} for 600 cycles.

To our knowledge, this is the best rate performance reported to date for both lithium and sodium storage in tungsten-sulfide materials. The exceptional electrochemical performance of our designed WS_2@G hybrids is thought to be the result of their unique structural and compositional features. Specifically, the space inside the hollow nanotubes can effectively accommodate the volumetric change of WS_2 upon electrochemical cycling [22]. The carbon shell not only improves the conductivity, but also prevents the WS_2 active materials from being eroded by direct contact with the electrolyte, resulting in a long cycle life [30–32]. The 1D structure is able to promote vectoral ion and electron transport, enabling the fast lithium storage [33]. Additionally, the nanosized WS_2 and the defect of the graphitic carbon coating with high surface area lead to a higher discharge capacity. Moreover, the interconnected self-supported film not only provides the most efficient electron transport pathways and forms a robust skeleton framework, but also increases the actual energy density without the addition of any other auxiliary component (e.g., binder, conductive carbon, foils).

CONCLUSIONS

In summary, we have successfully fabricated a novel 2D graphene/WS_2 hybrids by rolling 2D graphitic carbon into a hollow nanotube in which WS_2 nanoplates are encapsulated. When employed as a binder-free anode material, the composite exhibits excellent lithium and sodium storage properties for a rechargeable LIB or SIB cell, which is attributed to the external electronically conductive and elastic graphitic carbon nanotube networks as well as the surface carbon layer and the uniform distribution of WS_2 nanoplates. Considering the advantage and the universal characteristics of the 2D@2D hybrid structures, it can be easily extended to many applications in catalysis, gas-storage materials, sensors, and other electrochemical devices, especially for thin film devices.

Received 23 October 2017; accepted 18 December 2017; published online 12 January 2018

1 Cao X, Tan C, Zhang X, *et al.* Solution-processed two-dimensional metal dichalcogenide-based nanomaterials for energy storage and conversion. Adv Mater, 2016, 28: 6167–6196
2 Chhowalla M, Liu Z, Zhang H. Two-dimensional transition metal dichalcogenide (TMD) nanosheets. Chem Soc Rev, 2015, 44: 2584–2586
3 Huang X, Tan C, Yin Z, *et al.* Hybrid nanostructures based on two-dimensional nanomaterials. Adv Mater, 2014, 26: 2185–2204
4 Kong D, He H, Song Q, *et al.* Rational design of MoS_2@graphene nanocables: towards high performance electrode materials for lithium ion batteries. Energ Environ Sci, 2014, 7: 3320–3325
5 Yang Y, Fei H, Ruan G, *et al.* Vertically aligned WS_2 nanosheets for water splitting. Adv Funct Mater, 2015, 25: 6199–6204
6 Chhowalla M, Shin HS, Eda G, *et al.* The chemistry of two-dimensional layered transition metal dichalcogenide nanosheets. Nat Chem, 2013, 5: 263–275
7 Radisavljevic B, Radenovic A, Brivio J, *et al.* Single-layer MoS_2 transistors. Nat Nanotech, 2011, 6: 147–150
8 Meng R, Jiang J, Liang Q, *et al.* Design of graphene-like gallium nitride and WS_2/WSe_2 nanocomposites for photocatalyst applications. Sci China Mater, 2016, 59: 1027–1036
9 Yang X, Li Q, Hu G, *et al.* Controlled synthesis of high-quality crystals of monolayer MoS_2 for nanoelectronic device application. Sci China Mater, 2016, 59: 182–190
10 Wang Y, Kong D, Shi W, *et al.* Ice templated free-standing hierarchically WS_2/CNT-rGO aerogel for high-performance rechargeable lithium and sodium ion batteries. Adv Energ Mater, 2016, 6: 1601057
11 Li J, Shi X, Fang J, *et al.* Facile synthesis of WS_2 nanosheets-carbon composites anodes for sodium and lithium ion batteries. ChemNanoMat, 2016, 2: 997–1002
12 Huang G, Liu H, Wang S, *et al.* Hierarchical architecture of WS_2

nanosheets on graphene frameworks with enhanced electrochemical properties for lithium storage and hydrogen evolution. J Mater Chem A, 2015, 3: 24128–24138
13 Yang W, Wang J, Si C, *et al.* [001] Preferentially-oriented 2D tungsten disulfide nanosheets as anode materials for superior lithium storage. J Mater Chem A, 2015, 3: 17811–17819
14 Bhandavat R, David L, Singh G. Synthesis of surface-functionalized WS_2 nanosheets and performance as Li-ion battery anodes. J Phys Chem Lett, 2012, 3: 1523–1530
15 Lin S, Yang Z, Yue H, *et al.* Ridge-like Ni supported WS_2 films for lithium storage application. Mater Lett, 2015, 158: 9–12
16 Zhang L, Fan W, Liu T. Flexible hierarchical membranes of WS_2 nanosheets grown on graphene-wrapped electrospun carbon nanofibers as advanced anodes for highly reversible lithium storage. Nanoscale, 2016, 8: 16387–16394
17 Liu Y, Wang W, Wang Y, *et al.* Homogeneously assembling like-charged WS_2 and GO nanosheets lamellar composite films by filtration for highly efficient lithium ion batteries. Nano Energ, 2014, 7: 25–32
18 Liu Y, Wang W, Huang H, *et al.* The highly enhanced performance of lamellar WS_2 nanosheet electrodes upon intercalation of single-walled carbon nanotubes for supercapacitors and lithium ions batteries. Chem Commun, 2014, 50: 4485–4488
19 Seo JW, Jun YW, Park SW, *et al.* Two-dimensional nanosheet crystals. Angew Chem Int Ed, 2007, 46: 8828–8831
20 Yu S, Jung JW, Kim ID. Single layers of WS_2 nanoplates embedded in nitrogen-doped carbon nanofibers as anode materials for lithium-ion batteries. Nanoscale, 2015, 7: 11945–11950
21 Oumellal Y, Rougier A, Nazri GA, *et al.* Metal hydrides for lithium-ion batteries. Nat Mater, 2008, 7: 916–921
22 Xu X, Liu W, Kim Y, *et al.* Nanostructured transition metal sulfides for lithium ion batteries: Progress and challenges. Nano Today, 2014, 9: 604–630
23 Youn DH, Jo C, Kim JY, *et al.* Ultrafast synthesis of MoS_2 or WS_2-reduced graphene oxide composites *via* hybrid microwave annealing for anode materials of lithium ion batteries. J Power Sources, 2015, 295: 228–234
24 Shiva K, Ramakrishna Matte HSS, Rajendra HB, *et al.* Employing synergistic interactions between few-layer WS_2 and reduced graphene oxide to improve lithium storage, cyclability and rate capability of Li-ion batteries. Nano Energ, 2013, 2: 787–793
25 Lv W, Li Z, Deng Y, *et al.* Graphene-based materials for electrochemical energy storage devices: Opportunities and challenges. Energ Storage Mater, 2016, 2: 107–138
26 Zou M, Jiang Y, Wan M, *et al.* Controlled morphology evolution of electrospun carbon nanofiber templated tungsten disulfide nanostructures. Electrochim Acta, 2015, 176: 255–264
27 Du Y, Zhu X, Si L, *et al.* Improving the anode performance of WS_2 through a self-assembled double carbon coating. J Phys Chem C, 2015, 119: 15874–15881
28 Tarascon JM, Armand M. Issues and challenges facing rechargeable lithium batteries. Nature, 2001, 414: 359–367
29 Wang B, Li X, Qiu T, *et al.* High volumetric capacity silicon-based lithium battery anodes by nanoscale system engineering. Nano Lett, 2013, 13: 5578–5584
30 Goodenough JB. Energy storage materials: A perspective. Energ Storage Mater, 2015, 1: 158–161
31 Kong D, Li X, Zhang Y, *et al.* Encapsulating V_2O_5 into carbon nanotubes enables the synthesis of flexible high-performance lithium ion batteries. Energ Environ Sci, 2016, 9: 906–911
32 Kong D, He H, Song Q, *et al.* A novel SnS_2@graphene nanocable network for high-performance lithium storage. RSC Adv, 2014, 4: 23372–23376
33 Zheng Z, Gan L, Zhai T. Electrospun nanowire arrays for electronics and optoelectronics. Sci China Mater, 2016, 59: 200–216
34 Wang H, Kong D, Johanes P, *et al.* $MoSe_2$ and WSe_2 nanofilms with vertically aligned molecular layers on curved and rough surfaces. Nano Lett, 2013, 13: 3426–3433
35 Berkdemir A, Gutiérrez HR, Botello-Méndez AR, *et al.* Identification of individual and few layers of WS_2 using Raman Spectroscopy. Sci Rep, 2013, 3: 1755
36 Wang B, Li X, Zhang X, *et al.* Adaptable silicon–carbon nanocables sandwiched between reduced graphene oxide sheets as lithium ion battery anodes. ACS Nano, 2013, 7: 1437–1445
37 Li X, Song Q, Hao L, *et al.* Graphenal polymers for energy storage. Small, 2014, 10: 2122–2135
38 Li H, Yu K, Fu H, *et al.* Multi-slice nanostructured WS_2@rGO with enhanced Li-ion battery performance and a comprehensive mechanistic investigation. Phys Chem Chem Phys, 2015, 17: 29824–29833

Acknowledgements This work was supported by the Ministry of Science and Technology of China (2012CB933403), the National Natural Science Foundation of China (51425302, 51302045 and 5170021056), Beijing Municipal Science and Technology Commission (Z121100006812003), the Opening Project of State Key Laboratory of Advanced Technology for Float Glass, and the Chinese Academy of Sciences.

Author contributions Kong D and Qiu X designed and engineered the samples; Wang B, Xiao Z, Gao Y helped to carry out the characterization; Kong D wrote the paper with support from Zhi L and Yang Q-H. All authors contributed to the general discussion.

Conflict of interest The authors declare no conflict of interest.

Supplementary information Supporting data are available in the online version of the paper.

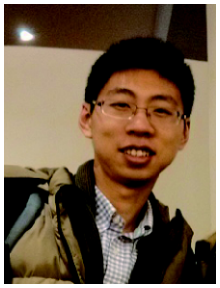

Debin Kong received his BSc and PhD in applied chemistry from Tianjin University under the guidance of Prof. Linjie Zhi and Prof. Quan-Hong Yang. Now he continues his scientific research as an Assistant Professor in the National Center for Nanoscience and Technology. His research interests mainly focus on the design and fabrication of novel carbon nanostructure and novel electrode materials for energy conversion and storage.

Xiongying Qiu received his bachelor's degree from the University of Chinese Academy of Sciences. He is currently an Engineer at the National Center for Nanoscience and Technology of China. His research interests mainly focus on graphene based materials and engineering research of energy storage device.

Quan-Hong Yang was born in 1972, joined Tianjin University as a full professor of nanomaterials in 2006 and became a chair professor in 2016. His research is related to novel carbon materials, from porous carbons, tubular carbons to sheet-like graphenes with their applications in energy storage and environmental protection. See http://nanoyang.tju.edu.cn for more details.

Linjie Zhi received his PhD in 2000 at the Institute of Coal Chemistry, CAS. Since 2003 he had been working with Prof. Müllen at Max-Planck Institute for Polymer Research for two years before assuming the position of project leader there until the end of 2007. He is currently a professor at the National Center for Nanoscience and Technology of China. His research interests focus on carbon-rich materials and their application in energy-related areas.

具有高电化学性能WS_2纳米片嵌石墨化纳米碳管材料(WS_2@G)用于锂离子或钠离子电池储能领域研究

孔德斌[1,2†], 邱雄鹰[1†], 王斌[1], 肖志昌[1], 张兴豪[1], 郭瑞莹[1], 高扬[1,2], 杨全红[2*], 智林杰[1*]

摘要 本论文通过结构设计及简单方法成功制备一种二维石墨烯-WS_2复合结构, 即WS_2纳米片嵌入石墨烯化中空纳米碳管中(WS_2@G). 这种新的电极结构采用静电纺丝技术和化学气相沉积技术组合的方式, 有利于实现集成化和无粘结剂锂离子或钠离子电池电极材料制备. 采用内部的受限生长以及原位的石墨化碳包覆纳米同轴的互贯网络, 得到纳米尺度WS_2片层分散的WS_2@G复合结构, 能够提供有效的导电性和电解液浸润性的网络结构, 同时还能够有效地降低电池在充放电循环过程中导致的体积膨胀效应, 最终实现一种高机械性能、无粘结剂、优异电化学活性的电极在锂离子或钠离子电池储能领域中的应用.

